

ABUAD Journal of Engineering Research and Development (AJERD) ISSN (online): 2645-2685; ISSN (print): 2756-6811



Volume 8, Issue 3, 134-147

Synthesis and Application of Starch-Modified Chitosan-Silver Nanoparticle Composite as Green Corrosion Inhibitor for Mild Steel in Acidic Media

Anthonia Fidamilare FIDUDUSOLA, Sylvia IGBAFE, Anselm Iuebego IGBAFE

Department of Chemical and Petroleum Engineering, Afe Babalola University, Ado-Ekiti, Ekiti State, Nigeria anthoniafidudusola@gmil.com/igbafesylvia@gmail.com/igbafeai@abuad.edu.ng

Corresponding Author: igbafeai@abuad.edu.ng,

Received: 06/09/2025 Revised: 16/10/2025 Accepted: 25/10/2025

Available online: 01/11/2025

+2348066596180

Abstract: The corrosion of mild steel in acidic environments presents a significant challenge across various industries, including oil and gas, chemical processing, and manufacturing. Traditional corrosion inhibitors, while effective, often contain toxic and environmentally harmful chemicals, prompting the need for sustainable alternatives. In this study, a novel—green corrosion inhibitor composed of cassava starch-modified chitosan and silver nanoparticles (AgNPs) was synthesized, characterized and application for protecting mild steel in dilute hydrochloric acid medium. The study utilized starchy extracts from waste cassava peel with chitosan synthesized from snail shells combined with green synthesis of AgNPs using phytochemicals of starch extracts as a reducing and stabilizing agent to formulate a biopolymer composite inhibitor. The starch, chitosan, and AgNPs formulation blend was varied in ratios, and inhibition effectiveness evaluated through gravimetric analysis, electrochemical measurements, and surface characterization techniques such as Fourier transform infrared spectroscopy, x-ray diffraction, and scanning electron microscopy. Findings, demonstrated that the starch-chitosan-AgNPs composite exhibited superior corrosion inhibition efficiency, reaching up to 97% at optimal starch concentrations. It also revealed that higher starch concentrations improved the inhibitor's performance due to increased surface coverage and adhesion. The inhibitor functioned by forming a protective film on the mild steel surface. The incorporation of AgNPs enhanced the inhibitor's stability and barrier properties, while the biopolymers provided biodegradability and non-toxicity. This work highlights the potential of biopolymer-based green inhibitors as sustainable alternatives to conventional corrosion inhibitors.

Keywords: Starch-Chitosan-AgNp Composite, Corrosion Inhibitor, Mild Steel, Acidic Environment, Green Corrosion Inhibitor

1. INTRODUCTION

The corrosion of metals, particularly mild steel, in acidic environments poses significant challenges across various industries, including construction, manufacturing, petroleum and natural gas surface and underground pipelines and crude oil refining, chemical and petrochemical processing [1,2]. Acidic solutions, such as those containing hydrochloric or sulfuric acids, are often used for processes like pickling, descaling, and industrial cleaning. However, these environments accelerate the degradation of mild steel, leading to reduced structural integrity, economic losses, and potential safety hazards [3]. To mitigate corrosion, the use of corrosion inhibitors has become a common practice. Traditional corrosion inhibitors such as chromates, nitrates, nitrites, and molybdates often involve synthetic chemicals that are toxic, and environmentally harmful. The move towards more sustainable practices has demanded for further eco-friendly and improve inhibition effective alternatives The application of green corrosion inhibitors such as plant-based, biopolymer-based, green nanomaterials and natural compounds, derived from natural or renewable resources, has gained significant attention due to their biodegradability, non-toxicity, and efficiency [4].

1.1 Biopolymer in Corrosion Inhibition

Biopolymer-based inhibitors have emerged as promising alternatives due to their biodegradability, non-toxicity. Chitosan, a natural polysaccharide and biopolymer derived from chitin, has received significant attention as a corrosion inhibitor due to its high molecular weight, film-forming ability, and active functional groups that promote strong adsorption onto metal surfaces [5]. However, its poor solubility in acidic media limits its effectiveness. To enhance its performance, chitosan can be modified with other biopolymers and functionalized with nanoparticles [6,7]. In addition, cassava starch, a natural polysaccharide, is widely used in industrial applications due to its biodegradability, water retention properties, and film-forming ability [8]. Consequently, the combination of cassava starch with chitosan can improve the inhibitor's solubility, adhesion, and protective properties, enhancing its efficiency in acidic environments. Additionally, starch acts as a complexing agent, promoting the uniform dispersion of chitosan on metal surfaces [9].

1.2 Nanoparticles in Corrosion Inhibition

Nanotechnology has further revolutionized corrosion inhibition by introducing metal nanoparticles. Syntheses are either by conventional chemical reduction methods or green methods. Unlike conventional chemical reduction methods

that involve toxic reducing agents, green synthesis utilizes natural polymers or plant extracts to reduce metal ions into nanoparticles, minimizing environmental pollution. Silver nanoparticles are well known for their antimicrobial, catalytic, and electronic properties, and recently as potential as corrosion inhibitors due to their ability to adsorb onto metal surfaces, forming protective layers that reduce corrosion rates [10]. The green synthesis of silver nanoparticles with phytochemicals of plant extracts to reduce silver ions into nanoparticles provides a sustainable, cost effective and eco-friendly approach.

Among known biopolymers, chitosan combined with starch offer excellent film-forming and surface-binding capabilities, it is important to examine evidence on their combined efficiency, stability, and synergistic behaviour when applied to mild steel in HCl media with silver nanoparticles which gives barrier qualities and antibacterial benefits Thus, this study aim was to synthesise a composite biopolymer of chitosan–starch–AgNPs as corrosion inhibitor for improved inhibition performance on mild steel in acidic medium.

2. THEORETICAL BACKGROUND

Corrosion manifests in a variety of forms, each with distinct characteristics, mechanisms, and implications for material performance.

2.1 Corrosion Types

Types include uniform or general corrosion the most common and widely recognized forms. It occurs evenly across the entire exposed surface of a metal and is typically caused by consistent exposure to a corrosive environment [11]. Pitting corrosion, a highly localized and problematic in stainless steels used in marine or chloride-rich environments. It compromises structural integrity of metal from pits formed [12,13]. Crevice corrosion, occurs in confined spaces such as gap between two metal surfaces, washers where stagnant conditions prevail [14]. Galvanic corrosion occurs when two dissimilar metals are in electrical contact within a conductive environment [11,15]. The intergranular corrosion targets the grain boundaries between alloy microstructures, rather than the grains such as in improperly heat-treated stainless steels [16]. Stress corrosion cracking combines mechanical stress with a corrosive environment to cause cracking and at stress levels below the material's yield strength a sudden failure of a component occur [17]. Erosion corrosion arises from the combined effects of mechanical wear and chemical attack where the protective films in metal piping systems, elbows or pumps with fluids in motion at high velocity [18]. Similar to erosion is cavitation corrosion, in which the metal surface protective coatings are removed due to localized shock waves from forceful collapse of vapor bubbles in a liquid near a metallic material [19]. Such repetitive mechanical action weakens the surface, leading to pitting and structural damage over time [20]. Others are high temperature corrosion which occurs due to exposure to hot environments containing reactive gases [21]. Microbiologically influenced corrosion are microorganisms, especially bacteria, influenced corrosion processes with sulphate-reducing bacteria as one commonly observed form [22].

2.2 Corrosion and Mechanism on Mild Steel

Corrosion is the deterioration of metal by a chemical attack or reaction with its environment. It is a constant and continuous problem, often difficult to eliminate completely. Corrosion processes develop fast after disruption of the protective barrier and are accompanied by a number of chemical reactions that change the composition and properties of both the metal surface and the local environment [23]. Corrosion occurs when metals react chemically or electrochemically with its environment which leads to the gradual and even loss of metal thickness over time [24]. Mild steel is low carbon content steel which lack alloying elements making it vulnerable to corrosion when exposed to acidic environments. Acidic solutions contain a high concentration of hydrogen ions (H⁺), which readily participate in electrochemical reactions with the metal. When mild steel comes into contact with an acid, the iron atoms in the steel are oxidized to iron ions (Fe²⁺ or Fe³⁺) known as rust, releasing electrons that reduce hydrogen ions in the solution to hydrogen gas. This reaction not only deteriorates the steel structure but also produces visible bubbles of hydrogen on the surface [25,26], illustrated as equations (1) to (4):

$$Fe \rightarrow Fe^{2+} + 2e^{-} \tag{1}$$

$$2H + 2e^- \rightarrow H2\uparrow$$
 (2)

$$O_2 + 2H_2O + 4e^- \rightarrow 4OH^-$$
 (3)

Overall reaction:
$$2\text{Fe} + \text{O}_2 + 2\text{H}_2\text{O} \rightarrow 2\text{Fe} \text{ (OH)}_2 \rightarrow \text{Fe}_2\text{O}_3 \cdot \text{xH}_2\text{O} \text{ (rust)}$$
 (4)

Mild steel corrodes rapidly in acidic settings due to the high concentration of hydrogen ions, which accelerates iron breakdown. If not managed effectively, this process results in material thinning, reduced mechanical strength, and eventual structural failure. Strong acids like hydrochloric acid (HCl) and sulphuric acid (H₂SO₄) are extremely harmful to mild steel and should not be stored in unprotected steel containers. Increased temperature, higher acid concentrations, contaminants, and dissolved oxygen all contribute to a faster corrosion rate [27].

2.3 Corrosion Inhibition on Mild Steel

Prevention would be more practical and achievable than complete elimination [11]. Several protective techniques are used to reduce corrosion in acidic conditions. Such as inhibitors, which adsorb onto the steel surface or form protective layers, preventing direct acid contact with the metal. Coatings such as paint, epoxy, or polymers form a physical barrier. Electrochemical approaches like cathodic protection. All mechanism remains based on economic feasibility, exposure

media, exposure length, and safety criteria. However, the use of corrosion inhibitors remains an inexpensive and effective method for control in aqueous and aggressive environments. The corrosion-inhibiting effect is attributed to the inhibitor's adsorption onto the corroding metal surface, thereby creating a barrier that isolates the metal from the corroding agents [28].

Chitosan is a natural biopolymer with an abundance of free amino groups synthesized through the deacetylation of chitin [29,30]. Its structure consists of β -1,4-linked glucosamine units, and its main properties and efficiency as a corrosion inhibitor are influenced by the degree of deacetylation (DD) and molecular weight [31]. The DD is extent of acetyl groups removal. Higher deacetylation leads to more amino groups. Rich amine and hydroxyl functional groups chitosan, promotes robust adsorption onto metal surfaces, generating protective layers that act as physical barriers against corrosive chemicals, which generally influences reactive and corrosion-inhibiting effectiveness [5, 32]. The molecular weight of chitosan is determined by the size of the polymer chains also affects the film-forming capacity and performance efficiency. Higher molecular weight chitosan typically providing better corrosion protection due to the increased number of functional groups available and surface area for adsorption onto metal surfaces [33,34]. Chitosan is more soluble in acidic solutions and can elevate the local pH near the metal surface, thereby limiting its effects in alkaline or neutral environment and lowering corrosion aggressiveness, except otherwise modified to derivatives like quaternized chitosan with sodium lauryl sulphate [35,36]. Consequently, crosslinked chitosan-based composite coating with inorganic salts, metals, or biopolymers can enhance the corrosion resistance by improving the film stability of the inhibitor [37-39]. Chitosan offers a sustainable and eco-friendly solution for applications in conditions requiring green corrosion management solutions [40].

Cassava (Manihot esculenta), is an abundant, low cost, root crop. Widely cultivated as food in tropical and subtropical regions as Africa, Asia, and South America, it is in rich starch content, comprising mainly amylose and amylopectin, it is natural source for biopolymers [40-42]. Starch, a repeating α-D-glucose units, is one most abundant natural semicrystalline biopolymer [43,44]. It is commercially available in plant roots or stems from maize wheat, potato and cassava [45,46]. Studies have recently explored starch as a supporting agent or composite material in corrosion inhibition as a filmforming agent or matrix for metal surfaces protection [47,48]. In aqueous solutions or gels, starch forms a viscous, adhesive film that can act as a physical barrier against oxygen, moisture on surfaces and reduces the rate of metal oxidation reactions [49]. Although, starch offers moderate inhibition properties on its own, its protective films can be significantly enhanced through chemical or physical modification, or by incorporating active inhibitory substances or nanoparticles [50-53]. The modification increases solubility, adhesion, and interaction with metal surfaces to improve its performance as a corrosion inhibitor through oxidation, etherification, and esterification by which the molecules form stronger bonds with the metal surface, improving their protective effect [43]. One of the most promising nanomaterials in corrosion inhibition is AgNPs. Ranging from 1 to 100 nanometres it contributes to corrosion inhibition through physical barrier formation and electrochemical interference. This physical barrier reduces both anodic and cathodic reactions for corrosion as a cathodic inhibitor, it slows down both the oxidation of the metal (anodic reaction) and the reduction of environmental oxidizers like oxygen (cathodic reaction). However, in combination with biopolymers the overall performance is enhanced [10,54,55]. In a composite system, AgNPs are dispersed uniformly throughout the polymer, creating a nanostructured coating inhibiting corrosion and antimicrobial protection in environments of harsh industrial wastes and marine processes disturbed microbial-induced corrosion [7,10,56,57,58].

3. METHODOLOGY

3.1 Materials

Cassava peel from ABUAD farm, Snail shells from Ado Ekiti open market, inorganic reagents of 97.0% NaOH, 36.5% HCl, 99.0% AgNO3 were all of Analar grades, purchased from industrial chemicals suppliers (Merck and fishersci), 99.85% CH3COOH, ACS grade from commercial suppliers of sigma Aldrich/Aefaemer),

3.2 Equipment

AV264 Electronic weigh balance, Ohaus, China, SKU:11-210 Water bath, HEMC equipment, India, Super-Nuova+Hot plate, ThermoScientific, UK, GCE Series Oven, Scots Ice, Australia, 5910 Ri Centrifuge, Eppendorf, Germany.

3.3 Starch Powder Preparation

Starch was recovered from waste cassava peels through a sequence of milling, suspension, filtration, and sedimentation procedures. The dried cassava peel was first ground and milled in a high-speed mixer for 5 minutes. The resultant powder was suspended in water at a 1:10 mass ratio, agitated for 5 minutes into a slurry paste, the slurry was filtered using cheesecloth. The filtrate was kept undisturbed for 2 hours to facilitate starch sedimentation. The supernatant was decanted and discarded, and the sediment was resuspended in fresh water at the same 1:10 ratio. The suspension was agitated for 5 minutes, and the operation was repeated three times to enhance starch purity. After the final sedimentation, the starch was isolated for further processing. The sediment was then dried at 55°C until a consistent weight was reached as described by Hasmadi and group [59].

3.4 Chitosan Preparation from Snail Shell

The snail shell was crushed into small parts using a mortar and pestle, then ground into fine particles. The ground powder was subjected to demineralization: 25 g of snail shell powder was immersed in 100 mL of 1 M HCl for 24 hours at room temperature. Thereafter, powder was rinsed with distilled water until a constant pH was obtained. The obtained

powder was sieved and dried in an oven at 60°C until a constant mass was attained before deproteinization. In deproteinization, the powder from demineralization was immersed in 1 M NaOH solution, followed by boiling in a water bath for 1 hour to remove protein. The mixture was afterwards, chilled at room temperature for 30 min, sieved, and rinsed with distilled water until it became neutral in pH. It was dried in the oven at 60°C until a constant mass was achieved to proceed for deacetylation. The deacetylation (partial removal of acetyl groups from chitin) was carried out by adding the dried powder to 10 M aqueous NaOH and boiled at 120°C for 2 hours on a hot plate. The mixture was allowed to cool for 15 minutes at room temperature. Thereafter, washed continually with distilled water to neutralize and filtered to keep its solid matter, which was the chitosan. The resulting chitosan was oven-dried at 60°C till a consistent mass was obtained [60].

3.5 Preparation of Green Silver Nanoparticles

A typical one-step synthesis method was applied by dissolving 1.0 g of soluble starch in 100 mL of deionised water, then slowly heating the mixture on a hot plate while stirring constantly. 50 mL of 1 mM silver nitrate solution was mixed with 10 mL of the starch solution, and the mixture was agitated for three hours on a hot plate to start the green synthesis of silver nanoparticles. The entire synthesis was done in complete darkness to avoid photochemical interference. The creation of nanoparticles was obtained by a discernible colour change from colourless to brownish-yellow, which was further verified by UV-visible spectroscopy. After thoroughly washing with distilled water, the resultant silver nanoparticles (AgNPs) were purified by repeated centrifugation at 1000 rpm for 1 hour. After purification, the AgNPs were re-dispersed in deionised water for characterization [61]. The measured XRD nanoparticle crystallite size was verified using the Scherrer equation, $D = K\lambda / (\beta \cos \theta)$, where D, is the estimate size, K, the shape factor (often around 0.9), λ is the X-ray wavelength, β is the full width at half maximum of the diffraction peak, and θ is the Bragg angle. This average size of the nano-crystallites is estimated by analyzing the broadening of XRD peaks, with smaller crystallites causing wider peaks [62].

3.6 Preparation of Chitosan-Starch Composite

Chitosan solution was formulated by dissolving 10 g of chitosan in 500 mL of a 1% (v/v) acetic acid solution. The solution was filtered via Whatman number 4-filter paper after the complete dissolution of chitosan. Then starch solutions with concentrations of 1%, 2%, 3%, and 4% (w/v) were formulated by dispersing pulverised cassava starch in distilled water, followed by boiling the mixtures on hotplates with continuous agitation until gelatinisation occurred. Thereafter, mixture was chilled to 25 °C. A chitosan-starch composite film was then synthesised by combining 100 mL of 2% chitosan solution with 100 ml of 0%, 1%, 2%, 3%, and 4% starch solutions as presented in Table 1 [63].

Sample	Composition (mixed ratios)
Blank	No inhibitor
A	100 mL (0% w/v) Starch: 100 mL (2% w/v) Chitosan: 20mL AgNp
В	100 mL (1% w/v) Starch: 100 mL (2% w/v) Chitosan: 20mL AgNp
C	100 mL (2% w/v) Starch: 100 mL (2% w/v) Chitosan: 20mL AgNp
D	100 mL (3% w/v) Starch: 100 mL (2% w/v) Chitosan: 20mL AgNp
\mathbf{E}	100 mL (4% w/v) Starch: 100 mL (2% w/v) Chitosan: 20mL AgNp

Table 1: Mixed ratios of composite inhibitor for corrosion test study

3.7 Preparation of Chitosan-Starch-Silver Nanoparticle Composite

20 mL of freshly synthesised green silver nanoparticle solution (1×10^{-3} M) was measured and gradually incorporated into the 1:1 formulated chitosan–starch solutions, at ambient temperature. The solutions were agitated constantly with magnetic stirrer for 2–3 hours to guarantee homogeneous distribution of the AgNPs throughout the biopolymer matrix. Following the mixing process, the composite was permitted to remain undisturbed for 2 hours at ambient temperature to achieve stabilisation [7].

3.8 Corrosion Test

Mild steel samples were cut into uniform rectangular coupons and polished using emery paper of varying grit sizes (400-1200) to obtain a smooth surface. After polishing, the samples were thoroughly washed with distilled water and ethanol to remove any surface contaminants, then dried and stored in a desiccator to prevent oxidation before use [56]. A solution of 1 M HCl received 200 mL treatment with various ratios of a starch, chitosan, and silver nanoparticle composite green inhibitor. Each inhibitor mixture contained a blank test sample using 1 M HCl alone as a reference control. The gravimetric analysis method served as the experimental approach for the study. The coupons underwent a predefined exposure period, then researchers removed them for cleaning, followed by drying until they obtained the weight loss information to determine corrosion amounts [2]. Corrosion rate and inhibition efficiency for each ratio of starch–chitosan–AgNPs were calculated using Equations (5) and (6).

Corrosion Rate (CR) =
$$\frac{87.6 \times \Delta W}{\rho \times A \times t}$$
 (5)

Where, ΔW is the weight loss on mild steel (mg), ρ is the density of mild steel (g/cm³), A is the surface area of the coupon (cm²), and t is the time of exposure (hr).

Inhibition efficiency (IE) =
$$\left(\frac{CR_{blank} - CR_{ratio}}{CR_{blank}}\right) \times 100$$
 (6)

Where, CR_{blank} is the corrosion rate in acid without inhibitor protect, and CR_{ratio} is the corrosion rate with specific ratio of starch–chitosan–AgNPs inhibitor mix.

4. RESULTS AND DISCUSSION

4.1 Characterisation of Starch

Figure 1(a), reveals functional groups in absorption band centred around 3282.89 cm⁻¹ corresponding to O–H stretching vibrations, indicating a strong hydrogen bonding from hydroxyl groups present in starch and polysaccharide and reflects extensive inter- and intramolecular hydrogen interactions. The hydroxyl groups present in starch molecules allow it to bond with other active corrosion inhibitors, creating a more robust and versatile protective film [64]. The moderate peak at 2930.76 cm⁻¹ is assigned to C–H asymmetric stretching vibrations of –CH₂ groups, confirming the presence of aliphatic chains within the starch backbone.

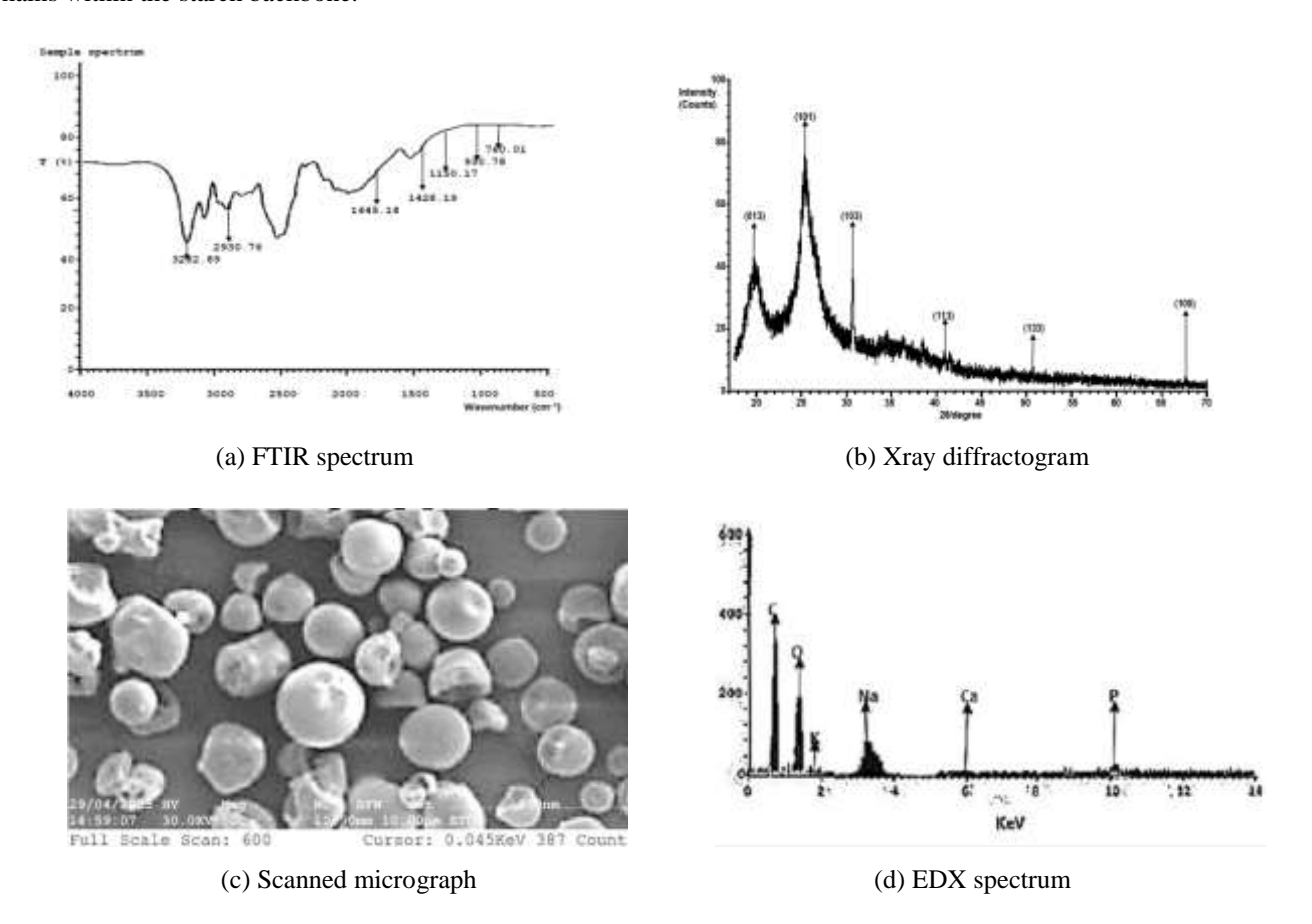


Figure 1: Topological, structural and elemental properties of produced starch

Crosslinked covalent bonds between starch molecules of starch coatings have also been found to improve adhesion to metal surfaces, making them more durable and effective at preventing corrosion [65]. The peak observed at 1645.18 cm⁻¹ is associated with H–O–H bending vibrations, likely due to absorbed water molecules, which are common in starch due to its hydrophilic nature. At 1428.19 cm⁻¹, CH₂ bending vibrations are evident, supporting the presence of methylene groups within the glucose units. A strong band at 1150.17 cm⁻¹ indicates C–O–C stretching vibrations related to glycosidic linkages, while the peak at 930.78 cm⁻¹ corresponds to skeletal vibrations of the glucose pyranose ring. The peak at 760.01 cm⁻¹ is attributed to ring deformation or C–H bending. The spectrum confirmed starch by the glycosidic bonds, hydroxyl functionality, and carbohydrate backbone integrity characteristic structural features. Figure 1(b), revealed detailed crystalline configuration of biopolymer of amylose and amylopectin, with distinct diffraction peaks at 20 values corresponding to planes (013), (101), (103), (113), (133), and (100), with the most intense peak observed at $2\theta \approx 25^{\circ}$ for the (101) plane. This dominant peak is indicative of significant crystallinity and may be associated with the B-type or C-type crystallinity typical of tuber starches like cassava. Crystallinity affects thermal stability, swelling capacity, solubility, and enzymatic digestibility, since film biodegradability performance is linked to crystalline structure. The sharpness and

intensity of the (101) peak suggest well-organized crystalline regions, while the broader peaks and sloping background indicate the presence of amorphous regions, which are due to the less ordered arrangement of starch molecules, particularly in amylose-rich zones. The (013) and partly (103) peaks at lower angles further confirm the presence of crystalline domains that contribute to the granular nature of native cassava starch. Higher-angle reflections, such as (113), (133), and (100), though of lower intensity, support the complex crystalline framework within the sample. These peaks provide evidence of multiplanar crystallographic reflections, confirming the polycrystalline structure. The relatively low baseline and moderate noise level suggest that the sample is primarily starch without significant impurities. This diffractogram indicates that the cassava starch exhibited semi-crystalline behaviour, which is typical of native starches. The starch morphology was characterized by oval, spherical, or truncated oval granules, with a particle size of 10.25 µm and a height of 14.17 µm, consistent with typical starch granule structures (Figure 1(c)). Elemental composition was dominated by carbon (48.21%) and oxygen (45.73%), which are primary components of starch's polysaccharide structure (Figure 1(d)). Trace elements such as sodium (2.21%), phosphorus (1.35%), potassium (1.00%), and calcium (1.50%) were also detected, likely originating from residual salts. Cationization enhances the starch electrostatic interaction with the negatively charged trace metal surfaces, improving its adhesion properties to form a protective layer and more suitable for long-term corrosion protection [66].

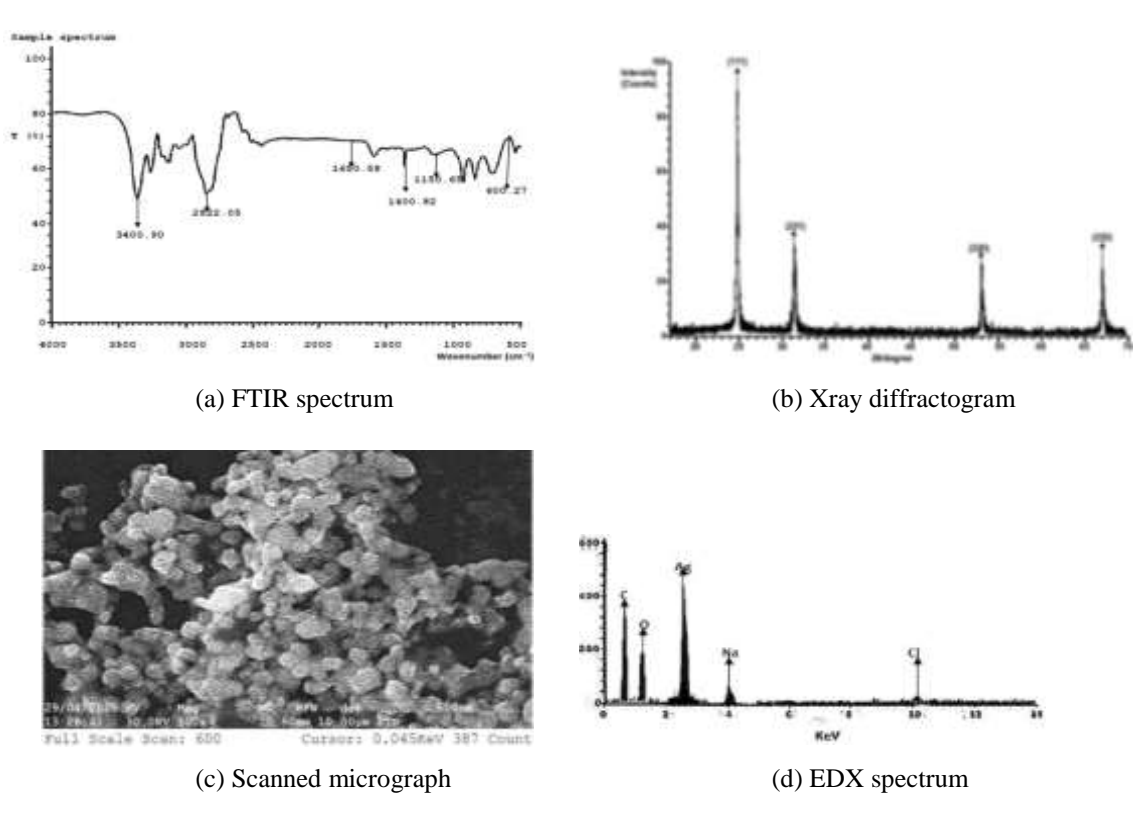


Figure 2: Topological, structural and elemental properties of synthesised AgNp

4.2 Characterisation of AgNp

In Figure 2(a), showed broad and strong absorption of the synthesized AgNPs, at 3400.90 cm⁻¹ corresponds to O–H stretching vibrations, indicating the presence of hydroxyl groups from polysaccharides (starch), which supplied the phytochemical reducing and capping agents during nanoparticle synthesis. This band also includes potential N–H stretching from proteinaceous compounds, further contributing to nanoparticle stabilization through hydrogen bonding or electrostatic interactions. A significant peak at 2922.05 cm⁻¹ attributed to C–H asymmetric stretching of –CH₂ groups, typical of aliphatic chains present in biopolymer stabilizers was noted. Also, a moderate band at 1650.58 cm⁻¹ is indicative of C=O stretching or C=C vibrations is present, which is often attributed to flavonoid or amide I groups, suggesting bioorganic compounds (phytochemicals) from the extract that were involved in capping the AgNPs. At 1400.82 cm⁻¹, the symmetric stretching of COO⁻ groups or CH₂ bending is evident, reflecting the presence of carboxylate groups that may interact with silver ions during synthesis. The absorption at 1150.65 cm⁻¹ corresponds to C–O stretching, representative of glycosidic linkages from the polysaccharide backbone, reinforcing the presence of starch or similar biomolecules. Notably, the low-wavenumber peak at 600.27 cm⁻¹ is associated with Ag–O or metal–oxygen bonds, confirming the formation of silver nanoparticles and their coordination with oxygen-containing groups. This metal-ligand interaction is essential in stabilizing the AgNPs. In Figure 2(b), the AgNPs exhibited characteristic peaks at 20 = 24.97° (111), 31.64° (231), and 53.26° (220), corresponding to the face-centred cubic crystal structure of metallic silver [67,68]. The sharp, well-defined

peaks indicate high crystallinity, while the absence of impurity peaks confirms phase purity. The crystallite size SEM observations of about 11 nm, aligned with the estimated 11.04 nm using Scherrer's equation [62]. Additionally, minor residual starchy peak (67.43°), confirming the organic capping agent's presence without disrupting the AgNPs' crystalline order.

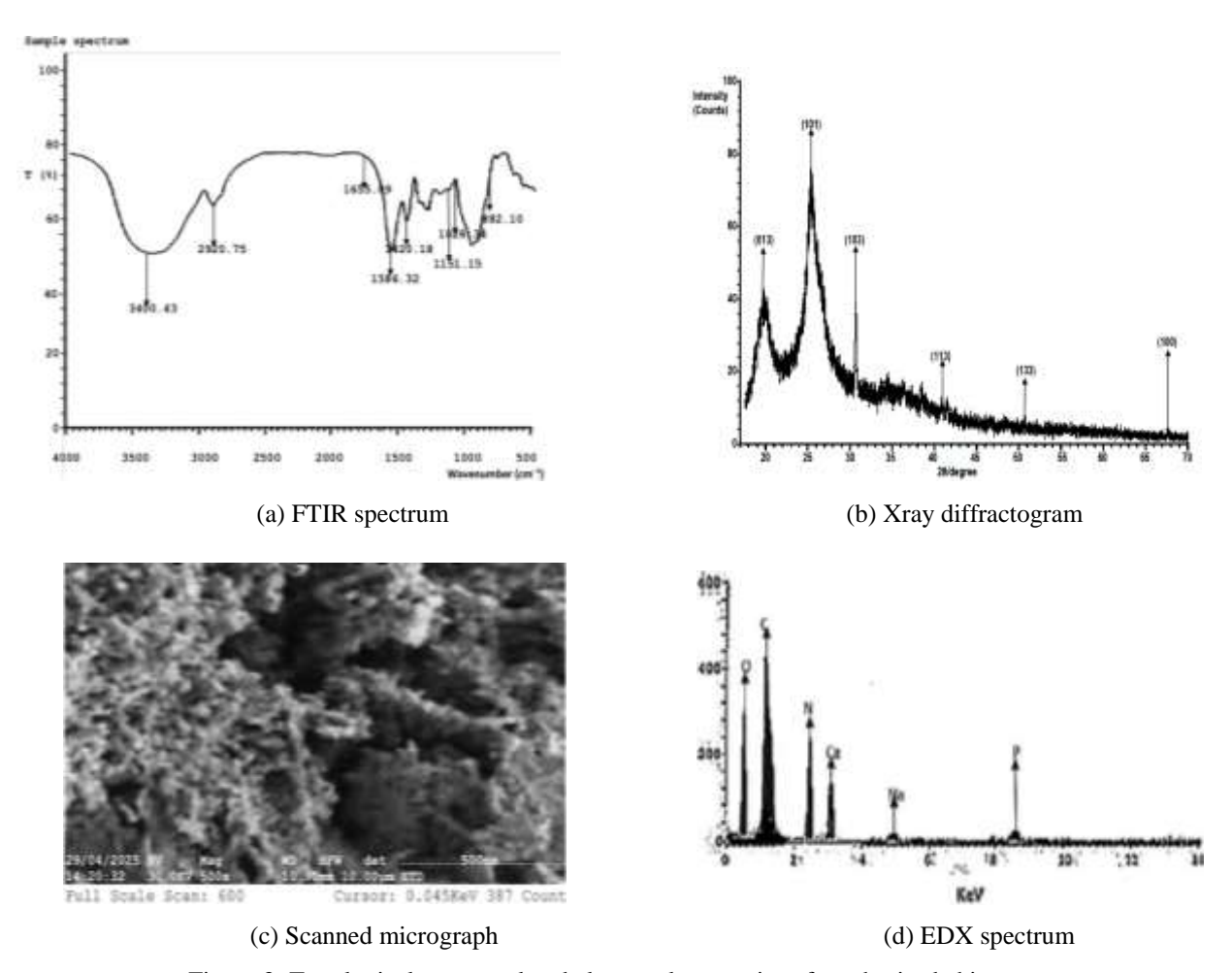


Figure 3: Topological, structural and elemental properties of synthesised chitosan

The morphology in Figure 2(c), shows uniform dispersion with minor irregularities due to aggregation or organic capping. It consists of mostly spherical and quasi-spherical particles, with an average size of 11.41 nm, likely influenced by the natural stabilizer (starch). While the spectroscopy of Figure 2(d), showed the elemental composition, with 65.23% silver, confirmed the metal nanoparticles, while carbon (21.47%) and oxygen (11.1%) indicated residual organics from the stabilizing matrix (starch). Trace elements such as sodium (1.25%) and chlorine (0.50%) were also detected as byproducts from the process synthesis.

4.3 Characterisation of Chitosan

Figure 3(a), shows a peak at 3400.43 cm⁻¹ (50.36%) due to overlapping O–H and N–H stretching, characteristic of chitosan's hydrophilic nature. The peak at 2920.75 cm⁻¹ (62.51%) indicates aliphatic C–H stretching and at 1655.09 cm⁻¹ (76.39%), a C=O stretch is seen, these are associated with residual acetyl groups from incomplete deacetylation. The amide II bands at 1586.32 cm⁻¹ (53.56%) shows N–H bending and C–N stretching, essential for chitosan's bioactivity. Peaks at 1420.18 cm⁻¹ and 1151.15 cm⁻¹ suggest methylene bending and glycosidic linkages, respectively. The presence of C–O stretching at 1028.34 cm⁻¹ and β-glycosidic linkages at 882.10 cm⁻¹ confirms its polysaccharide structure. In Figure 3(b), a semi-crystalline nature was observed, which is typical of this biopolymer. Prominent diffraction peaks were observed at 2θ values corresponding to planes (013), (101), (103), (113), (133), and (100). Among these, the (101) peak at around 25° is the most intense and sharp, indicating the dominant crystalline region in the chitosan structure, which arises from the orderly arrangement of polymer chains due to intermolecular hydrogen bonding. The broadness of some peaks, particularly at lower angle (013), suggests the coexistence of amorphous regions, reflecting partial disorder within the polymer matrix. This dual structure of crystalline and amorphous is crucial for the mechanical flexibility and biodegradability of chitosan. The additional peaks at higher angles, including (103), (113), (133) and (100), suggest a more defined and organized crystalline structure, which may result from specific preparation or treatment methods such as drying, deacetylation degree,

or molecular weight. The relatively low background intensity indicates low amorphous content, suggesting a higher degree of crystallinity than expected for typical chitosan. Figure 3(c), revealed a heterogeneous surface topography with visible granular features of irregular, flake-like morphology with porous and layered sheet-like structures, characteristic of its semi-crystalline biopolymer nature. While Figure 3(d) show elemental composition dominated by carbon (48.6%) and oxygen (35.95%), consistent with chitosan's polysaccharide structure. Trace elements such as nitrogen (8.59%), calcium (5.27%), and phosphorus (1.14%) were also detected, likely originating from residual salts or mineral impurities during treatment.

4.4 Characterisation of Chitosan-Starch-AgNPs Composite

In Figure 4(a), broad and intense absorption band observed around 3400.03 cm⁻¹ may be attributed to overlapping O–H and N–H stretching vibrations. This broadness indicates strong intermolecular hydrogen bonding between the hydroxyl groups of starch and the amino and hydroxyl groups of chitosan, suggesting effective blending and interaction between the two polymers. Such interactions play a critical role in enhancing the compatibility and mechanical integrity of the composite material. The absorption peak at 2920.54 cm⁻¹ corresponds to the asymmetric C–H stretching vibrations from – CH₂ groups, a common feature in the aliphatic backbones of both starch and chitosan. This peak confirms the presence of methylene structures, reinforcing the organic, chain-like nature of the composite. At 1654.32 cm⁻¹, the spectrum shows a distinct peak associated with C=O stretching vibrations, typically related to the amide I band. This can be attributed to residual N-acetyl groups in partially deacetylated chitosan, indicating the presence of some acetyl functionalities retained after processing. The chitosan's presence is again seen at 1550.00 cm⁻¹, where N–H bending vibrations occur, representing the amide II band. This peak is indicative of primary amine groups, reinforcing the contribution of chitosan's amino functionalities to the composite structure. The band at 1400.08 cm⁻¹ is associated with C–H bending vibrations, specifically from methylene and methyl groups, which are common in both polymers and contribute to the molecular flexibility and structural configuration.

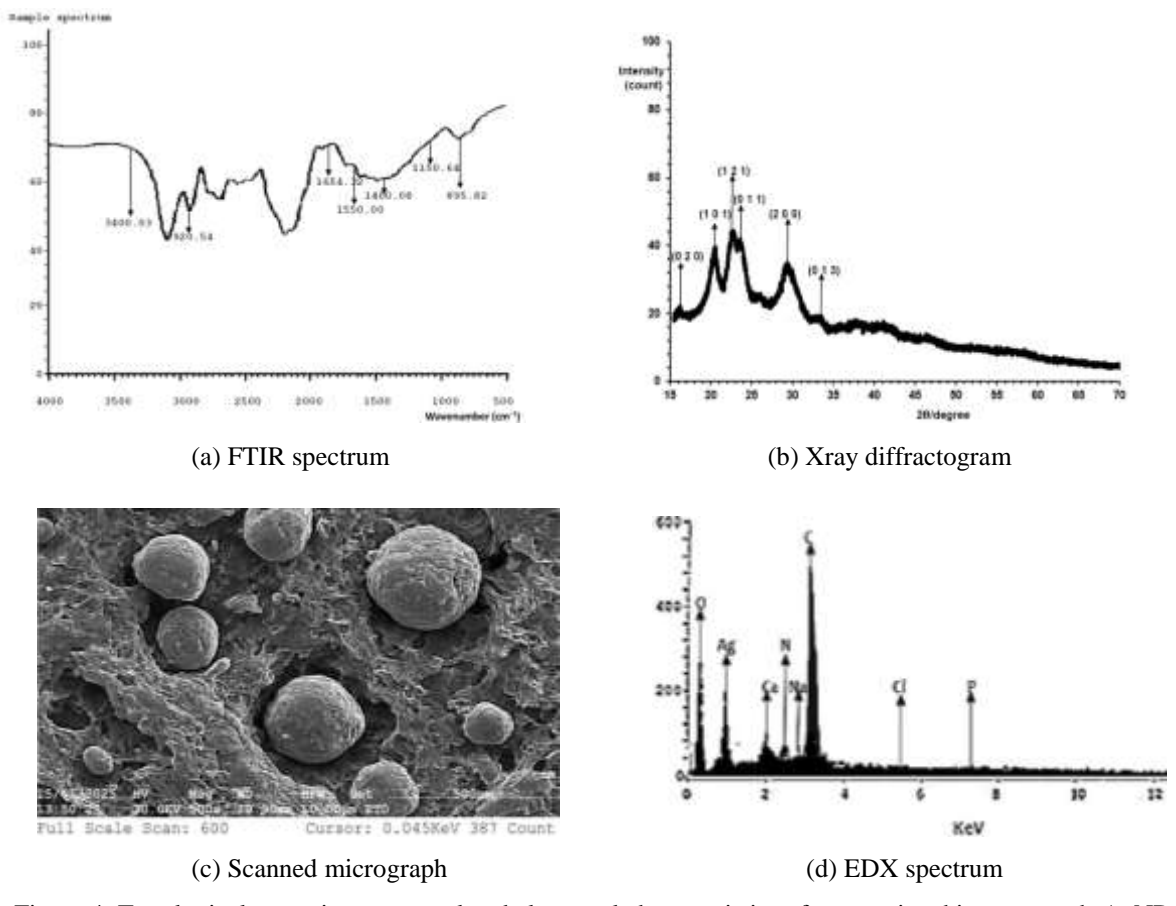


Figure 4: Topological, organics, structural and elemental characteristics of composite chitosan-starch-AgNPs

A prominent peak at 1150.64 cm^{-1} corresponds to C–O–C and C–O stretching vibrations, highlighting the presence of glycosidic linkages and the saccharide backbone, which are structural signatures of polysaccharides. Finally, the peak at 895.82 cm^{-1} informs the presence of β -glycosidic linkages, a hallmark of the polysaccharide structure, further validating the integrated blend. Figure 4(b) show distinct peaks at 2θ values corresponding to the crystal planes (020), (101), (121), (011), (200), and (013). These sharp peaks indicate the semi-crystalline nature of the composite, reflecting partial ordering

within the polymer matrix. Starch typically exhibits A-type, B-type, or C-type crystallinity, while chitosan generally shows broad peaks due to its amorphous or low-crystalline structure. The presence of several sharp peaks in this pattern, especially at lower angles (around 15°–30°), suggests that the starch component had significant contributions to the crystallinity of the composite material. Peaks such as (101) and (011) are characteristic of starch's crystalline domains, while minor shifts or broadening of peaks may indicate intermolecular interactions and partial disruption of crystalline regions due to blending with chitosan. The moderate peaks intensity is material partial crystallinity, while the broad background hump is presence of amorphous regions. This crystalline and amorphous phase can enhance the composite's biodegradability, flexibility, and film-forming properties. Figure 4(c) revealed a morphology of composite chitosan-starch-AgNPs, characterized by predominantly spherical particles with some irregular or quasi-spherical shapes due to a rough and heterogeneous surface, including visible starch inclusions. The particle size was measured at 35.41 μm with a height of 9.04 μm and a bulk density of 1.37 g/cm³. Figure 4(d) provided elemental composition, with significant peaks for carbon (42.57%) and oxygen (30.92%), consistent with the organic matrix of chitosan and starch. The presence of silver (14.23%) verified the incorporation of AgNPs, while trace elements like sodium (1.25%), chlorine (0.50%), calcium (1.09%), phosphorus (0.23%), and nitrogen (4.68%) were also detected, likely originating from residual salts or biomolecular components.

4.5 Surface Morphology of Mild Steel after Corrosion Test

In Figure 5(a), sample A (no inhibition), display a heterogeneous and highly irregular surface, with numerous uneven features. The microstructure appears disrupted suggesting a higher degree of surface deterioration. Which suggests effects of uncontrolled aggressive chemical exposures [69]. On another hand Figure 5(b), sample B (0% starch) revealed a pronounced strata-like surface texture with rough but layered morphology suggests that the surface has undergone substantial gully-like degradation, similar to erosion corrosion attack of flowing chemicals. The micrograph of Figure 5(c) of sample B (1% starch) revealed a significantly roughened and irregular surface similar to sample B but with evidence of loose surface microstructural particles and pitting indicative of localized corrosion attack. The introduction of starch may have enabled loose microstructure in particles.

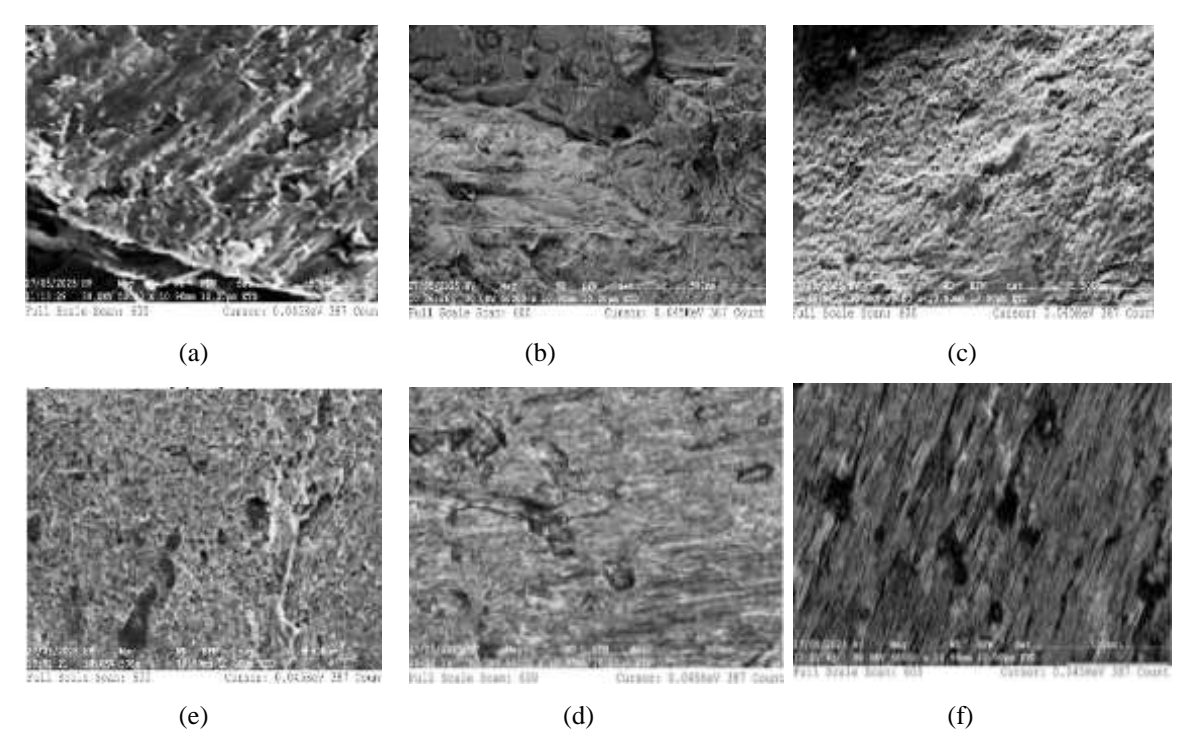


Figure 5: Morphology and elemental analyses of corroded mild steel sample surfaces

Figure 5(d) of sample C (2% starch) show distinct grooves and fibrous surface texture. The directional striations were indicative of corrosion propagation along the microstructural weak paths in the metal. Compared to sample B, the inhibitory effect on metal may have enabled a more structured degradation process. In Figure 5(e) of sample D (3% starch) reveals a surface with agglomerated fine particles and fairly regular pores, indicating minor corrosion and surface roughness. Figure 5(f) of sample E (4% starch) shows a densely agglomerated structure with a finer and more uniform particle distribution, indicating a relatively smoother and more compact surface. In all samples EDX analyses revealed iron content (48.25-61.82%), oxygen levels (27.05-36.11%) indicative of iron oxide as dominating product. Others as trace elements include sulphur (1.26-2.56%) as sulphides, chlorine (4.34-5.22%) as chlorides and silicon (3.11%) as silicates, while metals such as zinc (0.08-2.61%), sodium (0-3.32%) and aluminium (0-2.4%) and are present in moderate amounts,

consistent with alloying components or surface treatments. The metallic salts aid creation of composite coatings that provide superior protection against corrosion [46].

4.6 Corrosion Rate and Inhibition Efficiency

A distinctly declining trend with increasing starch concentration (0 to 4g) indicating degree of protective performance of was noticed for the corrosion rate against time profiles of the AgNP modified green composite biopolymer inhibitor (Figure 6). The blank sample, containing no inhibitor, exhibited the highest corrosion rate throughout the exposure period, confirming the aggressive nature of the acidic environment on unprotected mild steel.

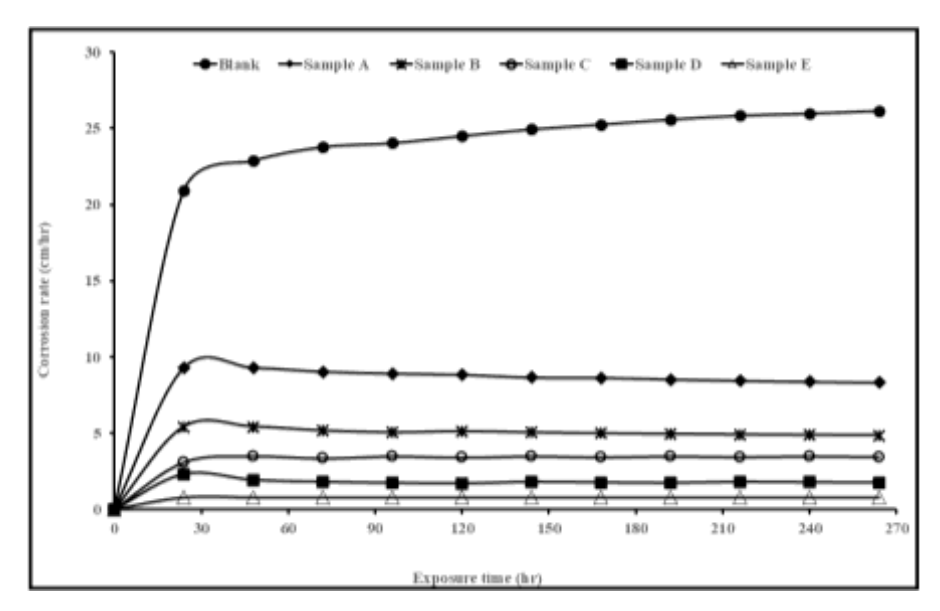


Figure 6: Corrosion rate against exposure time

Sample A, which contained only chitosan and silver nanoparticles without starch, showed a significant reduction in corrosion rate compared to the blank, highlighting the baseline protective ability of chitosan and AgNPs. As starch was introduced and increased from 1% to 4% a progressive decline in corrosion rate was observed. Sample E (4 w/v% starch) exhibited the most effective of inhibitor samples. This trend confirms that starch enhances the inhibitory performance of the chitosan–AgNPs composite. Thus, higher starch content enhanced the barrier layer on the metal surface, effectively reducing metal degradation in acidic media.

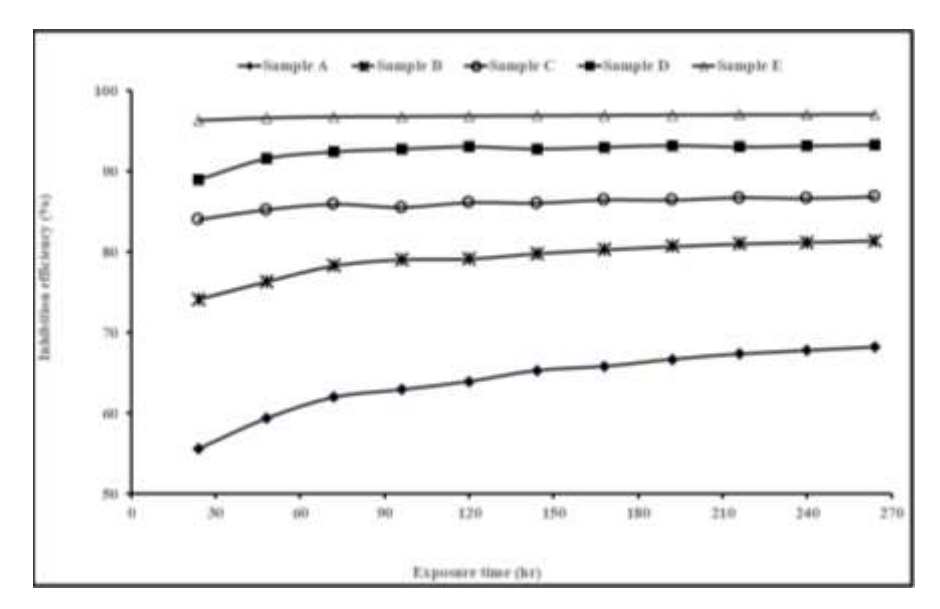


Figure 7: Inhibition efficiency against exposure time

The inhibition efficiency revealed an upward trend with increasing starch concentration, reflecting enhanced protective performance of the inhibitor system (Figure 7). Sample A exhibited moderate efficiency due to the combined action of chitosan and silver nanoparticles. However, the inclusion of starch solution in Samples B to E, significantly improved the efficiency, with Sample E (4% starch) achieving the highest inhibition efficiency of about 97.04%. The starch contributed

additional film-forming matrix and metal surfaces protection coverage, as well as improving the adherence and compactness of the protective layer on the mild steel [46]. Also, similar to observations documented in [52], increasing the starch content in the modified chitosan–AgNP matrix, further enhanced corrosion inhibition performance.

5. CONCLUSION

This study successfully synthesized and characterized a starch-modified chitosan-silver nanoparticle green inhibitor for mild steel in acidic media, demonstrating its effectiveness in reducing corrosion rates above 97%. The composite inhibitor leveraged the synergistic effects of chitosan's film-forming ability, starch's adhesive properties, and AgNPs' enhanced barrier and antimicrobial properties which often reduced the ability of microbial invasion. The inhibitor's eco-friendly nature, derived from renewable resources, positions it as a viable alternative to toxic synthetic inhibitors. The findings contribute to the advancement of eco-friendly materials in corrosion science, offering a cost-effective and environmentally benign solution for industrial applications. The study aligns with global sustainability goals by utilizing agricultural waste (cassava peel) and natural resources (snail shells), promoting a circular economy. The study underscores the importance of green chemistry in addressing industrial corrosion challenges while adhering to environmental sustainability principles.

ACKNOWLEDGEMENT

To all the academic staff in chemical and petroleum engineering, Afe Babalola university for the various expert advices provided on the study

REFERENCES

- [1] Groysman, A. S. (2017). Corrosion problems and solutions in oil refining and petrochemical industry, Koroze a Ochrana Materiálu, 61(3) 100-117, doi:10.1515/kom-2017-0013.
- [2] Jemini, E. T., Igbafe, S., Adeniyi, A. T., & Igbafe, A. I. (2024). Applications of green inhibitors of sugarcane bagasse and garcinia kola fruit pod for mild steel natural gas pipeline corrosion inhibition in acidic medium, Computational and Experimental Research in Materials and Renewable Energy, 7(2), 105-118, Doi.org/10.19184/cerimre.v7i2.50834
- [3] Manh, T. D., Huynh, T. H., Thi, B. V., Lee, S., Yi, J. & Dang, N. N. 2022). Corrosion inhibition of mild steel in hydrochloric acid environments containing sonneratia caseolaris leaf extract, ACS Omega. 7(10), 8874-8886. doi: 10.1021/acsomega.1c07237
- [4] Hamidi, N.A.S.M., Kamaruzzaman, W.M.I.W.M., Nasir, N.A.M., Shaifudin, M.S., & Ghazali, M.S.M. (2022). Potential application of plant-based derivatives as green components in functional coatings: A review, Cleaner Materials, 4, doi.org/10.1016/j.clema.2022.100097.
- [5] Ramasamy, P., Dubal, S.V., Jeyachandran, S., Pitchiah, S., Kannan, K., Elangovan, D., Thangadurai, T., Paramasivam, S., & Selvin, J. (2023). Control and prevention of microbially influenced corrosion using cephalopod chitosan and its derivatives: a review. International Journal of Biological Macromolecules, 242, 124924.
- [6] Ardean, C., Davidescu, C.M., Nemeş, N.S., Negrea, A., Ciopec, M., Duteanu, N., Negrea, P., Duda-Seiman, D., & Musta, V. (2021). Factors influencing the antibacterial activity of chitosan and chitosan modified by functionalization. International Journal of Molecular Sciences, 22(14), 7449, doi.org/10.3390/ijms2147449.
- [7] Hefni, H.H.H., Azzam, E.M., Badr, E.A., Hussein, M. & Tawfik, S.M. (2015). Synthesis, characterization and anticorrosion potentials of chitosan-g-PEG assembled on silver nanoparticles, International Journal of Biological Macromolecules, doi.org/10.1016/j.ijbiomac.2015.11.073.
- [8] Amaraweera, S.M., Gunathilake, C., Gunawardene, O.H., Fernando, N.M., Wanninayaka, D.B., Manamperi, A., Dassanayake, R.S., Rajapaksha, S.M., Gangoda, M., Fernando, C.A.N., & Kulatunga, A.K. (2021). Preparation and characterization of biodegradable cassava starch thin films for potential food packaging applications. Cellulose, 28, 10531-10548
- [9] Wan Yusof, W. R., Sabar, S., & Zailani, M. A. (2024). Starch-chitosan blends: A comprehensive review on the preparation, physicochemical properties and applications. Biopolymers, 115(5), e23602.
- [10] Raghavendra, N. (2024). Green silver nanoparticles/nanocomposite as a sustainable inhibitor to attenuate metal corrosion in hostile fluid environment: a review of recent developments, innovations and future opportunities. Journal of Bio-and Tribo-Corrosion, 10(4), 86.
- [11] Harsimran, S., Santosh, K., & Rakesh, K. (2021). Overview of corrosion and its control: A critical review. Proceedings on Engineering Sciences, 3(1), 13-24.
- [12] Aljibori, H. S., Alamiery, A., & Kadhum, A. A. H. (2023). Advances in corrosion protection coatings: A comprehensive review. International Journal of Corrosion Scale Inhibition, 12(4), 1476-1520.
- [13] Phull, B., & Abdullahi, A. A. (2017). Marine Corrosion. In: Reference Module in Materials Science and Materials Engineering. Oxford: Elsevier, 1-39, doi.org/10.1016/B978-044452787-5.00046-9.
- [14] Shifler, D. A. (2022). Localized Corrosion. LaQue's Handbook of Marine Corrosion, 63-121.
- [15]Katkar, V. A., & Gunasekaran, G. (2016). Galvanic corrosion of AA6061 with other ship building materials in seawater. Corrosion, 72(3), 400-412.
- [16]Malandruccolo, A. (2024). An Introduction to Stainless Steels. In Superaustenitic Stainless Steels: A Comprehensive Overview Cham: Springer Nature Switzerland, 1-71, doi.org/10.1007/978-3-031-68744-0.

- [17]Khalifeh, A. (2019). Stress corrosion cracking damages. Failure analysis, doi.org/10.5772/intechopen.80826.
- [18] Ayyagari, A., Hasannaeimi, V., Grewal, H. S., Arora, H., & Mukherjee, S. (2018). Corrosion, erosion and wear behavior of complex concentrated alloys: a review. Metals, 8(8), 603, doi.org/10.3390/met8080603
- [19]Skorb, E. V., Möhwald, H., & Andreeva, D. V. (2016). Effect of cavitation bubble collapse on the modification of solids: crystallization aspects. Langmuir, 32(43), 11072-11085.
- [20]Swain, B., Mohapatra, S. S., & Behera, A. (2021). Plasma spray coating: a weapon to fight with erosion and corrosion phenomena. In Thermal spray coatings, CRC Press, pp. 317-330.
- [21] Pedeferri, P., & Pedeferri, P. (2018). High temperature corrosion. Corrosion Science and Engineering, 589-610.
- [22] Javaherdashti, R., & Javaherdashti, R. (2017). Microbiologically influenced corrosion (MIC). Springer International Publishing, 29-79, doi.org/10.1007/978-1-84800-074-2.
- [23]Bender, R., Féron, D., Mills, D., Ritter, S., Bäßler, R., Bettge, D., De Graeve, I., Dugstad, A., Grassini, S., Hack, T., & Halama, M., (2022). Corrosion challenges towards a sustainable society. Materials and corrosion, 73(11),1730-1751.
- [24] Quadri, T. W., Akpan, E. D., Olasunkanmi, L. O., Fayemi, O. E., & Ebenso, E. E. (2022). Fundamentals of corrosion chemistry. In Environmentally sustainable corrosion inhibitors, 25-45, doi.org/10.1016/B978-0-323-85405-4.00019-7.
- [25] Avdeev, Y. G., & Kuznetsov, Y. I. (2021). Effect of iron (III) salts on steel corrosion in acid solutions. A review. International Journal of Corrosion and Scale Inhibition, 10(3), 1069-1109.
- [26]Klenam, D. E., Bodunrin, M. O., Akromah, S., Gikunoo, E., Andrews, A., & McBagonluri, F. (2021). Ferrous materials degradation: characterisation of rust by colour—an overview. Corrosion Reviews, 39(4), 297-311.
- [27]Li, L., Mahmoodian, M., Li, C. Q., & Robert, D. (2018). Effect of corrosion and hydrogen embrittlement on microstructure and mechanical properties of mild steel. Construction and Building Materials, 170, 78-90.
- [28] Aslam, R., Mobin, M., Zehra, S., & Aslam, J. (2022). A comprehensive review of corrosion inhibitors employed to mitigate stainless steel corrosion in different environments. Journal of Molecular Liquids, 364, 119992, doi.org/10.1016/j.molliq.2022.119992.
- [29] Iber, B. T., Kasan, N. A., Torsabo, D., & Omuwa, J. W. (2022). A review of various sources of chitin and chitosan in nature. Journal of Renewable Materials, 10(4), 42-49.
- [30] Novikov, V. Y., Derkach, S. R., Konovalova, I. N., Dolgopyatova, N. V., & Kuchina, Y. A. (2023). Mechanism of heterogeneous alkaline deacetylation of chitin: A review. Polymers, 15(7), 1729.
- [31] Hasan, S., Boddu, V. M., Viswanath, D. S., & Ghosh, T. K. (2022). Chitin and Chitosan. Science and Engineering; Springer Nature Switzerland: Cham, Switzerland, doi.org/10.1007/978-3-031-01229-7.
- [32] Novikov, V. Y., Konovalova, I. N., & Dolgopyatova, N. V. (2022). The mechanism of chitin and chitosan deacetylation during long-term alkaline treatment. Applied Biochemistry and Microbiology, 58(3), 309-314.
- [33] Binder, L., de Sousa Santos, F., & da Conceição, T. F. (2024). The influence of molecular weight on the anticorrosion properties of chitosan coatings. International Journal of Biological Macromolecules, 278, 134912.
- [34] Carrera, C., Bengoechea, C., Carrillo, F., & Calero, N. (2023). Effect of deacetylation degree and molecular weight on surface properties of chitosan obtained from biowastes. Food Hydrocolloids, 137, 108383.
- [35] Jessima, S. H. M., Berisha, A., & Srikandan, S. S. (2020). Preparation, characterization, and evaluation of corrosion inhibition efficiency of sodium lauryl sulfate modified chitosan for mild steel in the acid pickling process. Journal of Molecular Liquids, 320, 114382.
- [36] Wang, J. & Zhuang, S. (2022). Chitosan-based materials: Preparation, modification and application. Journal of Cleaner Production, 355, 131825.
- [37] Aguilar-Ruiz, A. A., Dévora-Isiordia, G. E., Sánchez-Duarte, R. G., Villegas-Peralta, Y., Orozco-Carmona, V. M., & Álvarez-Sánchez, J. (2023). Chitosan-based sustainable coatings for corrosion inhibition of aluminum in seawater. Coatings, 13(9), 1615, doi.org/10.3390/coatings13091615.
- [38] Das, A., Ghosh, S. & Pramanik, N. (2024). Chitosan biopolymer and its composites: Processing, properties and applications- A comprehensive review, Hybrid Advances, 6, doi.org/10.1016/j.hybadv.2024.100265.
- [39] El Ibrahimi, B., Guo, L., & Nardeli, J. V. (2021). The Application of Chitosan-Based Compounds against Metallic. In: Chitin and Chitosan: Physicochemical Properties and Industrial Applications, doi.org/10.5772/intechopen.96046.
- [40] Fetouh, H. A., Hefnawy, A., Attia, A. M., & Ali, E. (2020). Facile and low-cost green synthesis of eco-friendly chitosan-silver nanocomposite as novel and promising corrosion inhibitor for mild steel in chilled water circuits. Journal of Molecular Liquids, 319, 114355.
- [40] Kolawole, F. O., Kolawole, S. K., Olugbemi, O. M., & Hassan, S. B. (2019). Green corrosion inhibitory potentials of cassava plant (Manihot esculenta Crantz) extract nanoparticles (CPENPs) in coatings for oil and gas pipeline. In Corrosion inhibitors. doi.org/10.5772/intechopen.79221.
- [41] Nizzy, A. M., & Kannan, S. (2022). A review on the conversion of cassava wastes into value-added products towards a sustainable environment. Environmental science and pollution research, 29(46), 69223-69240.
- [42] Verma, C., Chauhan, D.S., Aslam, R., Banerjee, P., Aslam, J., Quadri, T.W., Zehra, S., Verma, D.K., Quraishi, M.A., Dubey, S., & AlFantazi, A. (2024). Principles and theories of green chemistry for corrosion science and engineering: design and application. Green Chemistry, 26(8), 4270-4357.
- [43] Wang, Z., Mhaske, P., Farahnaky, A., Kasapis, S., & Majzoobi, M. (2022). Cassava starch: Chemical modification and its impact on functional properties and digestibility, a review. Food Hydrocolloids, 129, 107542.

- [44] Sanders, J. M., Misra, M., Mustard, T. J. L., Giesen, D. J., Zhang, T., Shelley, J. & Halls, M. D. (2021). Characterizing moisture uptake and plasticization effects of water on amorphous amylose starch models using molecular dynamics methods, Carbohydrate Polymers, 252, doi.org/10.1016/j.carbpol.2020.117161.
- [45]Ahmad, M., Gani, A., Hassan, I., Huang, Q. & Shabbir, H. (2020). Production and characterization of starch nanoparticles by mild alkali hydrolysis and ultra-sonication process. Scientific Report, 10, 3533, doi.org/10.1038/s41598-020-60380-0.
- [46] Nsanzabera, F., Manishimwe, A., Mwiseneza, A., & Irakoze, E. (2023). Production of corn (zea mays) starch and cassava (manihot esculenta) starch and their application as yogurt stabilizer, Food and Nutrition Sciences, 14(7), 589-600. doi: 10.4236/fns.2023.147039.
- [47] AL Salihi, H. A., Mahdi, R. R., Al-Amiery, A., Al-Azzawi, W. K., & Kadhum, A. A. H. (2024). Exploring the efficacy of polysaccharides as green corrosion inhibitors: a comprehensive review. Starch-Stärke, 76(7-8), 2300234.
- [48] Huang, L., Chen, W. Q., Wang, S. S., Zhao, Q., Li, H. J., & Wu, Y. C. (2022). Starch, cellulose and plant extracts as green inhibitors of metal corrosion: a review. Environmental Chemistry Letters, 20(5), 3235-3264.
- [49] Majeed, T., Dar, A.H., Pandey, V.K., Dash, K.K., Srivastava, S., Shams, R., Jeevarathinam, G., Singh, P., Echegaray, N. & Pandiselvam, R. (2023). Role of additives in starch-based edible films and coating: A review with current knowledge. Progress in Organic Coatings, 181, p.107597.
- [50]Gamage, A., Punniamoorthy, T., & Madhujith, T. (2021). Starch-based hybrid nanomaterials for environmental remediation. In: Starch-Evolution and Recent Advances. doi.org/10.5772/intechopen.101697.
- [51] Navaf, M., Sunooj, K. V., Aaliya, B., Akhila, P. P., Sudheesh, C., Mir, S. A., & George, J. (2023). Impact of metal and metal oxide nanoparticles on functional and antimicrobial activity of starch nanocomposite film; A review. Measurement: Food, 11, 100099.
- [52] Quadri, T. W., Olasunkanmi, L. O., Fayemi, O. E., & Ebenso, E. E. (2023). Grafted Starch Used as Sustainable Corrosion Inhibitors. In: Grafted Biopolymers as Corrosion Inhibitors: Safety, Sustainability, and Efficiency, 313-335. doi.org/10.1002/9781119881391.ch14.
- [53]Yihang, Z. (2022). Application of water-soluble polymer inhibitor in metal corrosion protection: Progress and challenges. Frontiers in Energy Research, 10, 997107.
- [54]Zahran, M., Khalifa, Z., Zahran, M. A. H., & Azzem, M. A. (2021). Recent advances in silver nanoparticle-based electrochemical sensors for determining organic pollutants in water: A review. Materials Advances, 2(22), 7350-7365.
- [55] Zhao, Y., Zhang, Y., Dong, H., Wu, W., Yang, X., & He, Q. (2023). Functional biopolymers for food packaging: formation mechanism
- [56] Karmakar, B., Sarkar, S., Chakraborty, R., Saha, S. P., Thirugnanam, A., Roy, P. K., & Roy, S. (2024). Starch-based biodegradable films amended with nano-starch and tannic acid-coated nano-starch exhibit enhanced mechanical and functional attributes with antimicrobial activity. Carbohydrate Polymers, 341, 122321.
- [57]Ezzat, A. O., Aigbodion, V. S., Al-Lohedan, H. A., & Ozoude, C. J. (2024). Unveiling the corrosion inhibition efficacy and stability of silver nanoparticles synthesized using Anacardium occidentale leaf extract for mild steel in a simulated seawater solution. RSC advances, 14(26), 18395-18405.
- [58] Bamal, D., Singh, A., Chaudhary, G., Kumar, M., Singh, M., Rani, N., Mundlia, P., & Sehrawat, A.R. (2021). Silver nanoparticles biosynthesis, characterization, antimicrobial activities, applications, cytotoxicity and safety issues: An updated review. Nanomaterials, 11(8), 2086.
- [59]Hasmadi, M., Harlina, L., Jau-Shya, L., Mansoor, A. H., Jahurul, M.H A. & Zainol, M.K. (2021). Extraction and characterisation of cassava starch cultivated in different locations in Sabah, Malaysia, Food Research, 5(3), 44-52, doi:10.26656/fr.2017.5(3).550
- [60] Adeyi, A. A., Fasina, F. D., & Giwa, A. (2018). Kinetics and Isotherm Studies of liquid phase adsorption of cationic dye onto chitosan synthesized from crab shells. Journal of Engineering Research in Africa, doi.org/10.4028/www.scientific.net/jera.37.112.
- [61] Yakout, S. M. & Mostafa, A. A. (2015). A novel green synthesis of silver nanoparticles using soluble starch and its antibacterial activity, International Journal of Clinical and Experimental Medicine, 8(3), 3538-3544, PMCID: PMC4443080, PMID: 2606424
- [62] Monshi, A., Foroughi, M. & Monshi, M. (2012). Modified Scherrer equation to estimate more accurately nanocrystallite size using XRD. World Journal of Nano Science and Engineering, 2(3), 154-160. doi: 10.4236/wjnse.2012.23020.
- [63]Xu, Y. X., Kim, K. M., Hanna, M. A. & Nag, D. (2005). Chitosan-starch composite film: Preparation and characterization, Industrial Crops and Products, 21(2), 185-192, doi:10.1016/j.indcrop.2004.03.002
- [64]Umoren, S. A., and Eduok, U. M. (2016). Application of carbohydrate polymers as corrosion inhibitors for metal substrates in different media: A review. Carbohydrate polymers, 140, 314-341.
- [65] Nawaz, H., Waheed, R., Nawaz, M., & Shahwar, D. (2020). Physical and chemical modifications in starch structure and reactivity. In Chemical properties of starch. doi.org/10.5772/intechopen.88870.
- [66] Haroon, M., Wang, L., Yu, H., Abbasi, N.M., Saleem, M., Khan, R.U., Ullah, R.S., Chen, Q., & Wu, J. (2016). Chemical modification of starch and its application as an adsorbent material. RSC Advances, 6(82), 78264-78285.

- [67] Ali, M.H., Azad, M.A.K., Khan, K.A., Rahman, M.O., Chakma, U., & Kumer, A.(2023) Analysis of crystallographic structures and properties of silver nanoparticles synthesized using PKL extract and nanoscale characterization techniques. ACS Omega. 8(31), 28133-28142, doi:10.1021/acsomega.3c01261.
- [68] Todorova, M., Petrova, V., Ranguelov, B., Avdeev, G., Velkova, L., Atanasova-Vladimirova, S., Pisareva, E., Tankov, C., Tomova, A., Dolashki, A. & Dolashka, P. (2025) Green synthesis of antimicrobial silver nanoparticles (AgNPs) from the mucus of the garden snail cornu aspersum. Molecules. 30(10), 2150. doi: 10.3390/molecules30102150.
- [69]Gajdacsi, A., & Cegla, F. (2016). The effect of corrosion induced surface morphology changes on ultrasonically monitored corrosion rates. Smart Materials and Structures, 25(11), 115010.